Methods and Applications in Fluorescence

PAPER

Fluorescence monitoring of the effect of oxidized lipids on the process of protein fibrillization

RECEIVED
27 February 2016

REVISED
6 June 2016

ACCEPTED FOR PUBLICATION
22 June 2016

PUBLISHED
6 September 2016

Kateryna Vus[1,3], Rohit Sood[2], Galyna Gorbenko[1] and Paavo Kinnunen[2]

[1] Department of Nuclear and Medical Physics, V.N. Karazin Kharkiv National University, 4 Svobody Sq., Kharkiv 61022, Ukraine
[2] Department of Neuroscience and Biomedical Engineering, School of Science and Technology, Aalto University, FI-00076 Espoo, Finland
[3] Department of Nuclear and Medical Physics, V.N. Karazin Kharkiv National University, 12-38 Aeroflotska Str., Kharkiv 61031, Ukraine

E-mail: kateryna.vus@yahoo.com

Keywords: insulin fibrils, kinetics of amyloid formation, lysozyme fibrils, oxidized phospholipids, Thioflavin T

Abstract

The kinetics of lysozyme and insulin amyloid formation in the presence of the oxidized phospholipids (oxPLs) was investigated using Thioflavin T fluorescence assay. The kinetic parameters of fibrillization process (lag time and apparent rate constant) have been determined upon varying the following experimental parameters: the type of lipid assemblies (premicellar aggregates and lipid bilayer vesicles), pH, temperature and lipid-to-protein molar ratio. It was found that oxPLs premicellar aggregates induced the more pronounced increase of the maximum Thioflavin T fluorescence, which is proportional to the extent of fibril formation, compared to the vesicles composed of the oxidized and unoxidized lipids. In contrast, the oxPLs, used as dispersions or included into vesicles, inhibited fibril nucleation and elongation under near-physiological conditions *in vitro* compared to liposomes containing unoxidized lipids. The results obtained provide deeper insight into the molecular mechanisms of the oxidative stress-modulated conformational diseases, and could be employed for the anti-amyloid drug development.

1. Introduction

Fluorescence spectroscopy is currently one of the most informative and versatile tools for characterization of a wide variety of biological processes. Of these, the phenomenon of ordered protein aggregation (amyloid fibril formation) attracts particular interest due to its implication in molecular etiology of a number of so-called conformational disorders, including Alzheimer's, Parkinson's, Huntingtons diseases, type II diabetes, spongiform encephalophaties, etc [1, 2]. Amyloid fibrils are distinguished by a core cross-β-sheet structure in which polypeptide chains are oriented in such a way that β-strands run perpendicularly to the long axis of the fibril, while β-sheets propagate in its direction. One of the most sensitive and convenient criterion to differentiate between amyloid and other types of protein aggregates relies upon fluorescence measurement of benzothiazole fluorescent dye Thioflavin T (ThT) [3–5]. Specifically, kinetics of aggregation has been monitored *in vitro* by ThT fluorescence intensity, lifetime and anisotropy assays [6–8]. Furthermore, amyloid detection in tissue sections has been performed using fluorescence microscopy [9, 10]. The binding of ThT to amyloid fibrils is quite specific, followed by a several orders of magnitude fluorescence increase and red shift of the dye excitation spectrum [11]. This fluorophore belongs to a class of molecular rotors, possessing a strong quantum yield enhancement in viscous solvents [12, 13]. In aqueous solutions ThT quantum yield is very low (~0.0001), since relative rotation of the benzothiazole and benzylamine rings rapidly quenches the excited state [14]. On the contrary, ThT accommodation in the grooves running parallel to the fibril axis sterically block torsion relaxation upon excitation resulting in markedly enhanced fluorescence [15]. Notably, ThT is thought to associate with the grooves formed from at least five cross-strand residues, having the length ca. 15 Å, consistent with the dye size [11, 16]. For this reason, β-sheet surfaces found in native proteins are incapable of ThT binding, because they are typically three β-strands in width [17, 18].

Remarkable properties of ThT render this dye highly suitable for screening the inhibitors and modulators of amyloid self-assembly. While identifying the key factors modulating amyloid fibrillogenesis special attention is paid to membrane lipids. Growing

evidence indicates that lipid bilayer can promote amyloid nucleation through accumulation of the protein molecules adopting specific aggregation-competent conformation, orientation and location at the lipid-water interface [19, 20]. It has been hypothesized that anionic phospholipids represent the main membrane component responsible for the enhancement of fibril formation, as shown, particularly, for α-synuclein [21], Aβ peptide [22], amylin [23], tau [24], lysozyme, transthyretin, cytochrome c, insulin, myoglobin [25]. However, the observations that fibril formation *in vitro* can be induced not only by the membranes containing anionic phospholipids, but also by the bilayers composed of mixtures of zwitterionic phospholipids with gangliosides, sphingomyelin and cholesterol [26, 27], do not allow to attribute the ability to promote protein fibrillization to a certain class of lipids.

Of great interest in this context is the elucidation of the role of oxidized phospholipids (oxPLs) in modulating the fibril formation. The oxPLs formed upon peroxidation of the polyunsaturated phospholipids under the conditions of oxidative stress, are involved in the pathogenesis of several chronic diseases, including atherosclerosis and coronary artery disease [28, 29]. Specifically, oxidated low density lipoprotein, which accumulates in atherosclerotic lesions, has been found to promote thrombosis [30]. OxPLs are capable of triggering the immune response, inflammation and apoptosis in cells, the effects being attributed to the altered physical properties of these species compared with unoxidized lipids [31]. Interestingly, the properties of the hydrated oxPLs are similar to those of surfactants, because micelles and soluble pre-micellar complexes were identified at high and low oxPLs concentrations, respectively [32, 33]. Furthermore, an increase of their content in lipid vesicles to $\geqslant$20% is reported to promote the membrane pore formation [34]. Recent monolayer measurements suggest that oxPLs take the extended conformation due to arrangement of oxidatively modified lipid chains parallel to the membrane plane [35, 36]. Such a conformation can modify the bilayer polarity profile so that it no longer forms a barrier to the penetration of water [23]. Finally, phase separation in the lipid bilayers and decrease of the energy barrier for flip-flop were triggered by the oxPLs [37, 38].

Oxidative stress that induces lipid peroxidation has been associated with Alzheimer's and Parkinson's diseases due to its ability to promote Aβ peptide deposition, tau hyperphosphorylation and dopamine cell degeneration [39–41]. Furthermore, oxidation has been demonstrated to initiate fibrillization of Aβ peptide and α-synuclein [42, 43]. Interestingly, lipid peroxidation is accelerated by transition metal ions such as Fe^{2+} and Cu^{2+}, which were also found to modulate protein fibrillization [44, 45]. The above findings suggest that amyloid fibril formation could be triggered by the oxPLs. Indeed, the Aβ_{1-42}, amylin, and gelsolin fibrillization appeared to be much faster in the presence of membranes containing oxPLs compared to those formed from the unoxidized lipids [46–48]. Furthermore, it was demonstrated that 1-palmitoyl-2-(9′-oxononanoyl)-sn-glycero-3-phosphocholine accelerates fibril formation from the core amyloidogenic segment of gelsolin (residues 179–194) [10]. Interestingly, the Aβ_{1-40} fibrillization process was facilitated and spherical amyloid nuclei were generated due to increased hydrophobicity of the oxPLs-modified peptide [48]. According to the literature, the effect of oxPLs on amyloid fibrillization kinetics is 2-fold. First, covalent binding of oxPLs to histidine or cysteine residues results in Shiff base formation and protein cross-linking [49]. Second, surface polarity of the oxPLs-containing membranes is lower than that of the bilayers from nonoxidized phospholipids, so that polypeptides tend to maximize intramolecular hydrogen bonding by folding into α-helices, followed by their aggregation [46]. However, despite the substantial progress made in the study of amyloid formation on lipid membrane surfaces, clear understanding of the role of oxPLs in this process is lacking due to a very small number of the proteins investigated in this regard [50–52]. Notably, the membrane-mediated amyloidogenesis is closely linked to the toxicity of pre-fibrillar protein aggregates, because lipid-oligomer interactions trigger membrane pore formation followed by ion imbalance and cell death [52–55]. In view of this, more detailed studies of lipid effects on protein fibrillization kinetics and fibril morphology could provide necessary tools for drug development.

The present work was aimed at *in vitro* investigation of fibrillization kinetics of lysozyme and insulin in the presence of chemically designed oxPLs using Thioflavin T assay. More specifically, our goals were: (i) to uncover the effects of the oxPLs-containing liposomes or lipid dispersions on amyloid fibril formation at varying lipid composition, pH, temperature and ionic strength; (ii) to quantitatively characterize the kinetics of lipid-mediated protein fibrillization; (iii) to compare the roles of unoxidized phospholipids and oxPLs in amyloid fibril formation; (iv) to shed light on the molecular mechanisms of oxPLs-mediated amyloidogenesis.

2. Materials and methods

2.1. Materials

Hen egg white lysozyme, insulin from bovine pancreas and Congo Red were purchased from Sigma (St. Louis, MO, USA). Thioflavin T was from Molecular Probes (Oregon, USA). Stock solutions of the fluorophores were prepared by dissolving ThT and CR in 5 mM sodium phosphate buffer and ethanol, respectively. The dye concentration was determined spectrophotometrically using the extinction coefficients $\varepsilon_{412} = 23\,800$, $\varepsilon_{498} = 47\,000$, for ThT and CR, respectively. 1-palmitoyl-2-azelaoyl-sn-glycero-3-phosphocholine (PazePC), 1-palmitoyl-2-(9′-oxononanoyl)-sn-glycero-3-phosphocholine

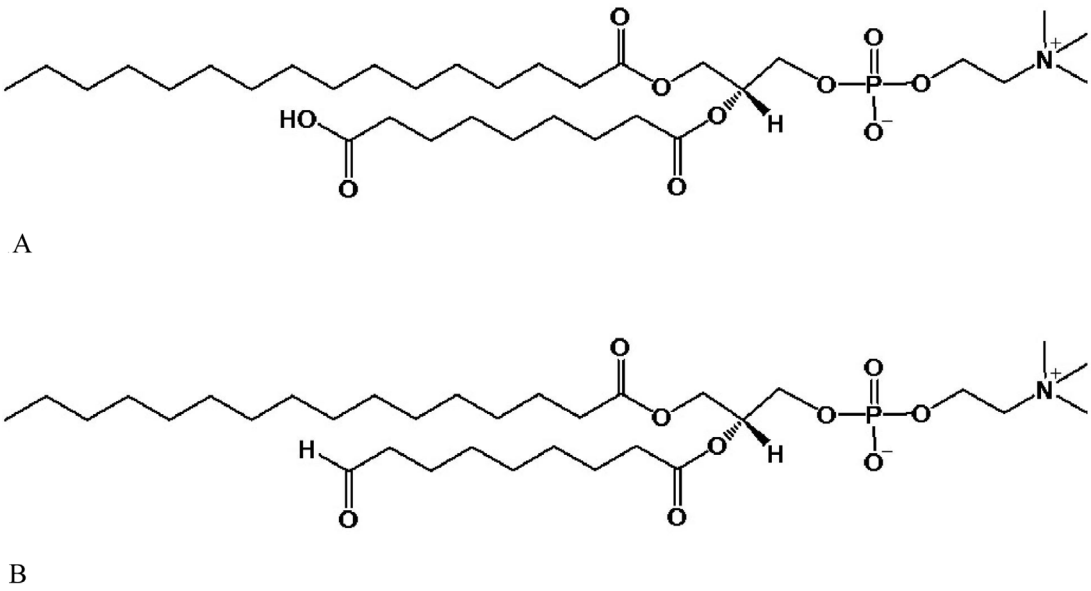

Figure 1. Structures of 1-palmitoyl-2-azelaoyl-sn-glycero-3-phosphocholine (PazePC) (A) and 1-palmitoyl-2-(9′-oxononanoyl)-sn-glycero-3-phosphocholine (PoxnoPC) (B).

(PoxnoPC), 1-hexadecanoyl-2-(9Z-octadecenoyl)-sn-glycero-3-phospho-(1′-rac-glycerol) (sodium salt) (PG) and 1-palmitoyl-2-oleoyl-sn-glycero-3-phosphocholine (PC) lipids were from Avanti Polar Lipids (Alabaster, AL). The structures of PazePC and PoxnoPC are shown in figure 1.

2.2. Preparation of lipid dispersions and vesicles

A certain amount of the lipid stock solution in chloroform was added to the glass tube and the solvent was removed under a stream of nitrogen. Next, the lipid residue was maintained under the reduced pressure for 4 h. The dry lipids were hydrated in 5 mM sodium phosphate or 10 mM glycine buffers. Furthermore, PazePC and PoxnoPC samples were placed in a bath sonicator for 1 h to obtain optically clear lipid dispersions (PazePC disp and PoxnoPC disp, respectively) [56]. Alternatively, AVESTIN LipoFast extruder (AVESTIN Inc., Canada) was used for preparing liposomes of the following composition: PC:PazePC (4:1, mol:mol); PC:PoxnoPC (4:1, mol:mol); PC:PG (4:1, mol:mol); PC, below referred to as $PazePC_{20}$, $PoxnoPC_{20}$, PG_{20} and PC, respectively. Lipid samples were extruded through a 50 nm pore size polycarbonate filter, and size of the vesicles was controlled by dynamic light scattering.

2.3. Steady-state fluorescence measurements

Steady-state fluorescence spectra of the dyes were recorded with Varian Cary Eclipse (Varian Instruments, Walnut Creek, CA) spectrofluorimeter equipped with a magnetically stirred, thermostated cuvette holder. Fluorescence measurements were performed using 10 mm path-length quartz cuvettes. The excitation and emission slit widths were set at 10 nm.

2.4. Kinetics of amyloid formation observed by Thioflavin T assay

For the kinetic studies the quartz cuvettes were filled with 2 ml of solutions (pH 1.6 or 7.4) containing the tested protein samples (1.6 and 16.4 μM of lysozyme and insulin, respectively), Thioflavin T (14 μM), 130 mM NaCl and different amounts of lipid (0, 1.6 or 16.4 μM). Notably, the oxPLs concentration in the cuvettes was below the critical micelle concentration (CMC) [32]. The obtained solutions were further incubated in the thermostated cuvette holder of the spectrofluorimeter at 37 or 60 °C under constant stirring. ThT was excited at 430 nm and the emission spectra were collected at 450–600 nm every 5–10 min. Typical surface plots, showing the ThT fluorescence as a function of the wavelength and time of lysozyme incubation in the presence of the oxPLs and in the control sample, are represented in figure 2. Quantitative characteristics of the fibrillization process were obtained using the approximation time (t) dependence of the ThT fluorescence intensity at 480 nm (F) with the sigmoidal curve [6]:

$$F = F_0 + \frac{F_{max} - F_0}{1 + \exp\left[k(t_m - t)\right]}, \qquad (1)$$

where F_0 and F_{max} are ThT fluorescence intensities dye in the free form and in the presence of protein after the saturation has been reached, respectively; k—apparent rate constant for the fibril growth; t_m—the time to 50% of maximal fluorescence. The lag time was calculated as: $t_m - 2/k$. The shift of the dye emission maxima ($\Delta\lambda_{max}$) was found as the difference between the wavelengths, corresponding to the highest intensity of ThT spectrum after the saturation of the fluorescence had been reached and that of the dye in the sample being tested before starting its incubation.

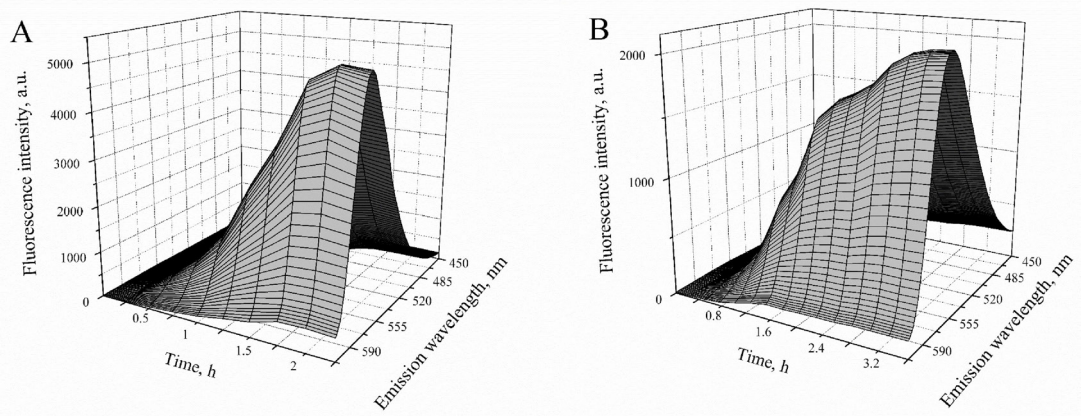

Figure 2. Surface plots, showing the ThT fluorescence as a function of the wavelength and time of lysozyme incubation at pH 1.6, 60 °C, 16 μM PazePC dispersions (A) and without lipid (B).

2.5. Transmission electron microscopy

For electron microscopy assay, a 10 μl drop of the protein solution (16 μM, taken from the tested sample after the fibril growth has been finished) was applied to a carbon-coated grid and blotted after 1 min. A 10 μl drop of 2% (w/v) uranyl acetate solution was placed on the grid, blotted after 30 s, and then washed 3 times by deionized water and air dried. The resulting grids were viewed at Tecnai 12 BioTWIN electron microscope.

2.6. Congo red assay

After the saturation of ThT fluorescence has been reached, the aliquots of the solutions (600 μM) used for the ThT kinetic studies were placed into 2 mm quartz cuvettes. Next, the absorbance of each sample was measured between 350 and 700 nm, followed by adding a drop of Congo Red stock solution to reach the dye concentration 48 μM. Absorption spectra of the tested solutions without CR and free dye were subtracted from those of the fluorophore-containing samples to get the difference spectra of CR. Notably, 130 μM lysozyme and 40 μM insulin were used to obtain clearly distinguishable peaks in CR spectra at 542 nm corresponding to the fibril-bound dye [57, 58].

2.7. Dynamic light scattering (DLS)

Zetasizer Nano ZS (Malvern Instruments, Malvern, UK) was used to measure DLS from liposome suspension in 1 cm cuvettes. Intensity scattering data were collected after a thermal equilibration time of 2 min. DLS data were reported as a volume based particle size distribution, and an average of 3 runs was calculated for each sample.

3. Results and discussion

Incubation of lysozyme and insulin solutions at low pH and/or elevated temperature typically results in amyloid fibril formation [59–62]. In view of this, to explore the effect of oxPLs on the protein fibrillization we used glycine (pH 1.6) or sodium phosphate (pH 7.4) buffers at two temperatures (60 °C and 37 °C). PC and PG_{20} vesicles were examined for comparison. The measurements were performed at lipid concentration 16 μM, whereas the most substantial effects of the oxPLs and lipid surfactants on gelsolin, ApoC-II and Aβ-peptide fibrillization were observed below the CMC [47, 56]. Likewise, ionic surfactants inhibited the protein fibrillization above the CMC at pH 7 [63]. As shown in figure 3(A), ThT fluorescence exhibits large increase with the time of lysozyme incubation at pH 1.6, 60 °C, lipid-to-protein molar ratio of 1:1, and varying composition of lipid vesicles/dispersions. Furthermore, positions of the dye emission maxima were shifted to the shorter wavelengths (table 1, $\Delta\lambda_{max}$), revealing a decrease in the environmental polarity of the protein-bound fluorophore. Kinetic analysis of the resulting sigmoidal curves indicate that the presence of $PazePC_{20}$/$PoxnoPC_{20}$ liposomes reduces the lag time for fibril formation compared to that of control lysozyme samples. In turn, protein association with PazePC/PoxnoPC dispersions result in the fluorescence enhancement, which is proportional to the extent of fibril formation (table 1). Analysis of the DLS data at the time point corresponding to the formation of mature fibrils showed that lysozyme interactions with oxPLs-containing bilayer trigger liposome disruption due to the increase of the average particle diameter by several orders of magnitude compared to that of freshly prepared vesicles (table 2). This could result from the oxPLs-induced membrane pore formation [37]. Notably, the observed changes in particle size cannot be attributed neither to the amorphous aggregates, since such a kind of structures has not been detected by TEM (figure 4), nor to the fibrils, because they typically have the average particle diameters *ca.* 1–100 nm [64, 65]. Inclusion of the oxPLs [44, 66] and PG [67] into PC bilayer leads to the increase in membrane hydration, decrease or increase of membrane polarity, respectively, compared to the neat PC vesicles. It appeared that at pH 1.6 and 60 °C membrane surfaces promote faster amyloid nucleation compared to that in a control sample, whereas protein interactions with the most hydrophobic bilayers (PC) give rise to

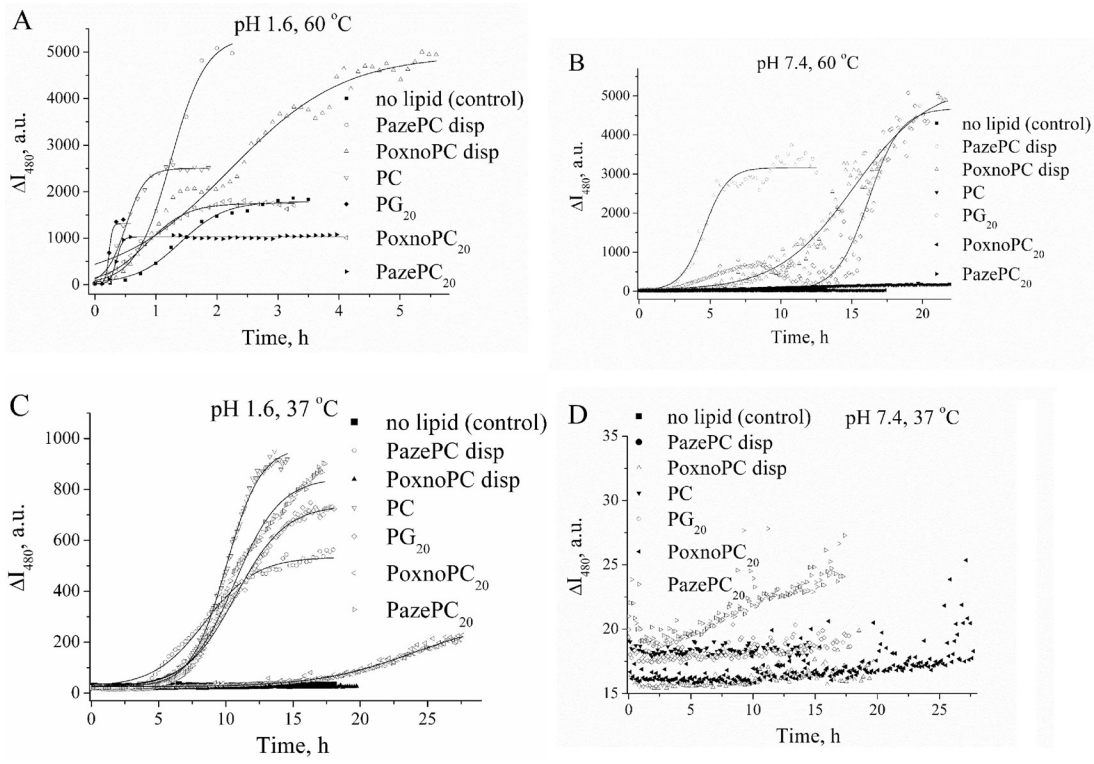

Figure 3. Kinetics of lysozyme fibrillization under different conditions. Lysozyme, lipid and ThT concentrations were 16.4, 16.4 and 14 μM, respectively.

Table 1. Kinetic parameters of lysozyme fibrillization in the presence of unoxidized and oxidized phospholipids.

Lipid type	pH	T (°C)	k (h^{-1})	Lag time (h)	F_{max} (a.u.)	F_{max}/F_0 (a.u.)	$\Delta\lambda_{max}$ (nm)
Control	1.6	60	2.7	0.7	1788	72	−5
PG_{20}			35	0.2	1315	53	−15
PC			6.3	0.2	2500	100	−13
$PazePC_{20}$			21.5	0.3	1029	42	−8
$PoxnoPC_{20}$			3	0.2	1750	70	−19
PoxnoPC disp			1.1	0.4	4935	198	−10
PazePC disp			3.5	0.7	5331	214	−12
Control	1.6	37	—	—	—	—	—
PG_{20}			0.5	6.7	752	31	−12
PC			0.8	7.4	968	39	−14
$PazePC_{20}$			0.6	7.3	847	34	−13
$PoxnoPC_{20}$			0.3	17	292	12	−12
PoxnoPC disp			—	—	—	—	—
PazePC disp			0.5	4.5	535	22	−6
Control	7.4	60	—	—	—	—	—
PG_{20}			0.9	14	4685	181	−8
PC			0.3	4.9	195	8	−21
$PazePC_{20}$			0.4	1.5	66	3	−10
$PoxnoPC_{20}$			—	—	—	—	—
PoxnoPC disp			0.4	9.7	5293	212	−20
PazePC disp			1.2	2.9	3166	127	−11

more pronounced extent of fibril formation (table 1). Furthermore, maximum fluorescence intensity of ThT in the presence of the oxPLs dispersions (F_{max}) was ~3 times greater than that in the control sample. The above data suggest that association with membrane surface accelerates lysozyme fibril nucleation, presumably due to the local increase in protein concentration, while the oxPLs dispersions probably enhance monomer denaturation, thereby favouring fibril formation [46]. Specifically, latter effect of the oxPLs could be caused

Table 2. Average particle diameters (D) and their percentage (%) in buffer solutions of liposomes and liposome–protein mixtures observed by dynamic light scattering.

T, pH	Liposomes (control)	PC	$PazePC_{20}$	$PoxnoPC_{20}$	PG_{20}
25 °C, 7.4	D (nm)	65	43	45	59
	%	93	96	98	99
T (°C)	Liposomes (+lysozyme)[a]	PC (pH 1.6)	$PazePC_{20}$ (pH 1.6)	$PoxnoPC_{20}$ (pH 1.6)	PG_{20} (pH 1.6)
37	D (nm)	1093	872	1264	798
	%	77	97	93	100
60	D (nm)	30	248	890	60
	%	99	97	90	100
T (°C)	Liposomes (+insulin)[a]	PC (pH 7.4)	$PazePC_{20}$ (pH 7.4)	$PoxnoPC_{20}$ (pH 7.4)	PG_{20} (pH 7.4/1.6)
37	D (nm)	39	43	42	33/63
	%	82	88	96	89/48
60	D (nm)	41	41	59	49/374
	%	96	82	95	70/98

[a] Liposome–protein mixtures were taken for analysis after finishing fibril growth.

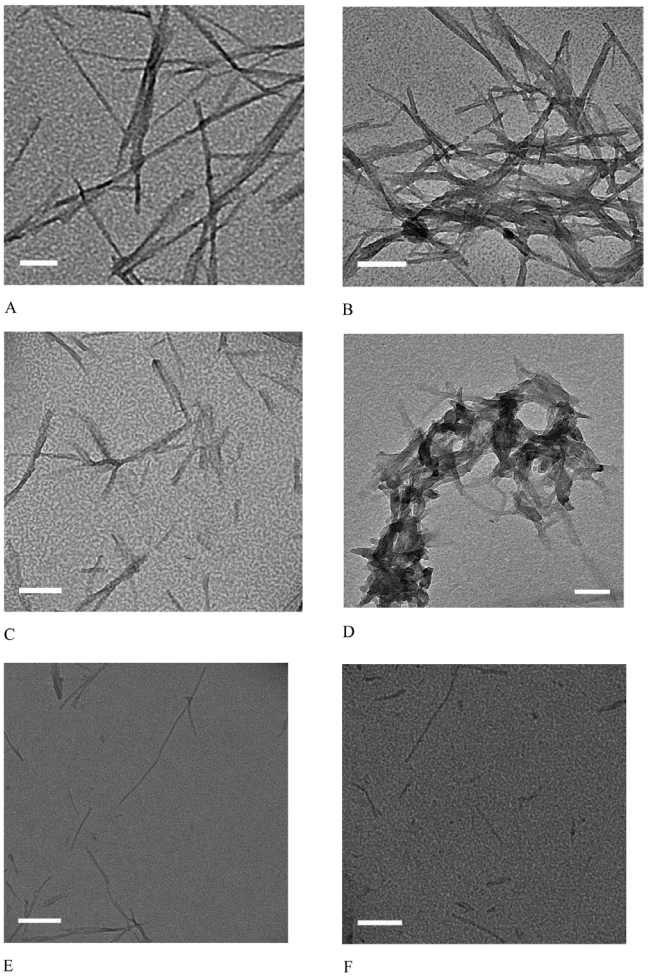

Figure 4. TEM images of lysozyme fibrils (16.4 μM) formed at pH 1.6, 130 mM NaCl, 60 °C in the absence (A) and presence (B) of 16 μM PazePC dispersions; at pH 1.6, 130 mM NaCl, 37 °C, 16 μM PazePC dispersions (C), and pH 7.4, 130 mM NaCl, 60 °C, 16 μM PazePC dispersions (D). Insulin fibrils (16.4 μM) formed at pH 7.4, 130 mM NaCl, 60 °C, 16.4 μM PazePC dispersions (E) and without lipid (F). Scale bars are 100 (A) and 200 ((B)–(F)) nm.

Table 3. Protein fibrillization (+) in the presence of oxidized and unoxidized phospholipids at varying pH and temperature revealed by ThT assay.

Protein	pH	T (°C)	PazePC disp	PoxnoPC disp	$PazePC_{20}$	$PoxnoPC_{20}$	PG_{20}	PC	Control
Lysozyme	1.6	60	+	+	+	+	+	+	+
	1.6	37	+	−	+	+	+	+	−
	7.4	60	+	+	−	−	+	−	+
	7.4	37	−	−	−	−	−	−	−
Insulin	1.6	60	+	+	+	+	+	+	+
	7.4	60	+	+	+	+	+	+	+
	7.4	37	+	+	+	+	+	+	+

by the formation of an amphiphilic 1:1 complex between lysozyme and PoxnoPC/PazePC premicellar aggregates, as has been demonstrated previously for Finnish mutant type D187N $gelsolin_{179–194}$ using tryptophan fluorescence quenching. Furthermore, below the CMC the coupling between PoxnoPC and gelsolin occurred via a Shiff base, resulting in the lipid embedding inlipid:proteinoligomers and fibrils [56]. However, the differences in the F_{max} could occur due to either the variations in lysozyme fibril morphology, or the changes in the extent of protein fibrillization [68].

At pH 7.4, 60 °C lysozyme has been shown to form amorphous aggregates [59], while fibril formation under these conditions was observed only in the presence of denaturants [69, 70]. Indeed, no fibrils were formed in buffer solution (figure 3(B)). Furthermore, the presence of membrane surfaces did not induce marked lysozyme fibrillization, except of PG_{20} that promoted *ca.* 181-fold increase of ThT fluorescence (table 1). These findings can be explained by the lowered pH of the membrane surface, whereas electrostatic interactions are not crucial at the lipid–protein ratio 1:1 [51, 71]. In turn, PoxnoPC dispersions induced the highest rate of lysozyme fibrillization compared to liposomes, in accordance with the results obtained at pH 1.6 and those reported previously for Finnish mutant type D187N $gelsolin_{179–194}$ [56]. It seems probable that the contribution of acidic pH to the formation of the aggregation-prone lysozyme conformation is more significant than the effect of lipids, because at pH 1.6 the lag times of lipid-modulated lysozyme fibrillization were 5–70 times lower and apparent rate constants were 3–54 times greater than those at pH 7.4 (table 1). However, the oxPLs dispersions induced a substantial increase in ThT fluorescence regardless of pH value. Furthermore, PoxnoPC premicellar aggregates accelerated lysozyme fibrillization at pH 7.4, with F_{max} values being higher than in the case of PazePC dispersions. The triggering and inhibiting effects of the lipids under study are summarized in table 3. The finding that oxPLs induce lysozyme fibrillization at neutral pH can provide deeper insight into the molecular mechanisms underlying lysozyme amyloidosis *in vivo*.

Another parameter strongly influencing the lipid-modulated protein fibrillization along with pH, is the incubation temperature (figures 3(C) and (D); table 1). Specifically, at pH 1.6, 37 °C a substantial decrease of k, F_{max}, and increase of the lag time of lysozyme fibrillization was observed compared to pH 1.6, 60 °C. Indeed, as follows from TEM data, elevation of incubation temperature from 37 °C to 60 °C results in the increase of the number of lysozyme fibrillar aggregates (figures 4 (A)–(C)). Notably, membrane surfaces promoted the accelerated protein fibrillization and greater values of F_{max} in comparison with the PazePC dispersions. In turn, in control samples and in the presence of PoxnoPC premicellar aggregates no fibrils were detected by ThT fluorescence assay. As mentioned above, PoxnoPC molecules have aldehyde and electrophilic carbonyl groups, which form covalent Michael adducts or Schiff bases due to the reactions with thiol and amino moieties [72]. Since the stability of the Schiff base decreases with temperature, one cannot exclude the stabilizing effect of PoxnoPC-lysozyme covalent interactions on the protein oligomers that reduce fibril formation [73]. Overalls, we found that only the oxPLs interactions with thermally denaturated lysozyme molecules (at 60 °C) result in fibril growth, whereas at pH 7.4, 37 °C no lipid-triggered fibril formation was detected, indicating that acidic pH and elevated temperature are essential prerequisites for lysozyme fibrillization *in vitro* [59, 60].

As seen in figures 4(A)–(D), lysozyme aggregates had the morphology of amyloid structures: they are unbranched, *ca.* 400 nm–1 μM in length and 20 nm–45 μM in width [5, 60]. Notably, the morphology of lysozyme fibrils forming in PazePC dispersion at pH 7.4, 60 °C, differs from that of aggregates observed at pH 1.6, 60 °C (figures 4(A) and (D)). The fibrils grown in the presence of PazePC dispersions were *ca.* 45 nm in diameter and had a flat-ribbon, smooth shape with a high degree of curvature, similar to the morphology of the fibrils formed from the β-sheet region of T4 lysozyme at 55 °C in 20% trifluoroethanol [74]. Furthermore, an increased degree of curvature was detected in lysozyme fibrils prepared at pH 1.6, 60/37 °C, 16 μM PazePC dispersions, compared to the morphology of aggregates grown at pH 1.6, 60 °C (figures 4(B) and (C)). In contrast, fibrils prepared at pH 1.6, 60 °C were *ca.* 25 nm in diameter and had a rod-like shape. Likewise, the effect of the oxPLs dispersions on lysozyme fibrillization resembles that of ethanol, as was reported previously [75]. Specifically, it was demonstrated in our

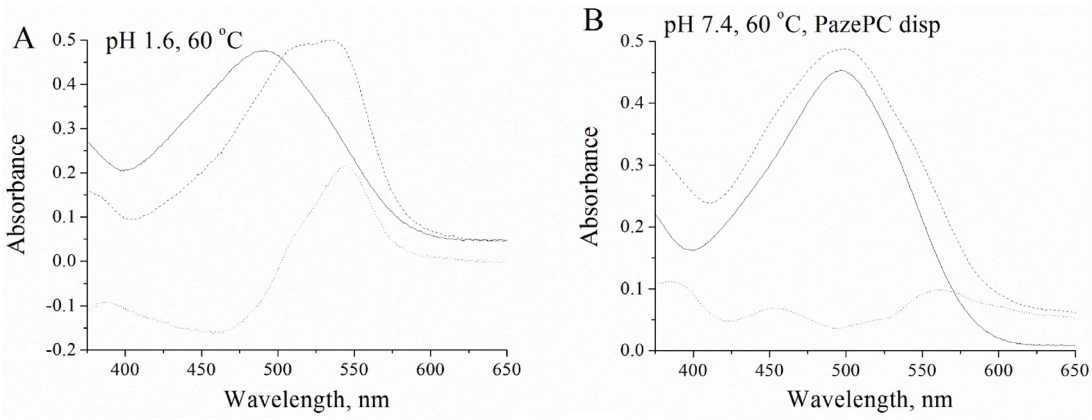

Figure 5. Absorption spectra of Congo Red (dashed lines) in the presence of fibrillar lysozyme formed at pH 1.6, 60 °C (A), or pH 7.4, 60 °C, PazePC dispersion (B). The spectra were corrected for light scattering due to fibrils. The dye and the protein concentrations were 48 and 120 μM, respectively. Solid lines correspond to the absorbance of free CR in buffer and dotted lines—to the difference spectra of CR.

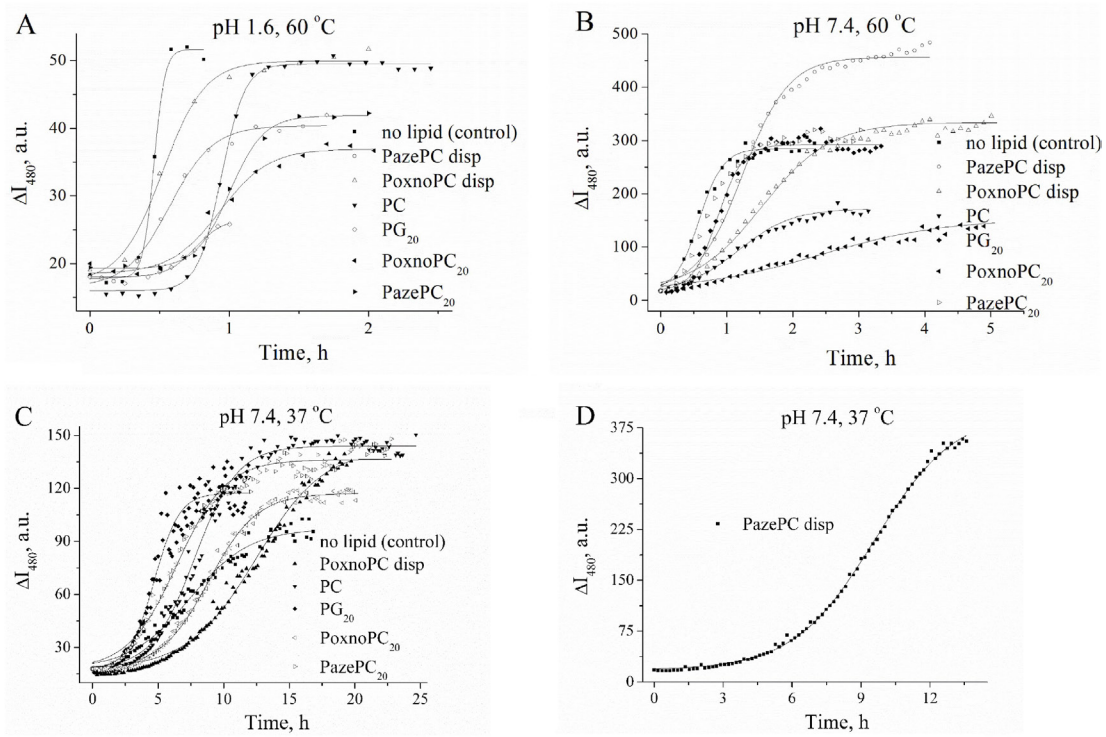

Figure 6. Kinetics of insulin fibrillization under different conditions. Insulin, lipid and ThT concentrations were 1.6, 16.4 and 14 μM, respectively.

previous studies that ThT showed a higher fluorescence increase when bound to the aggregates grown in 80% ethanol, pH 7.4, compared to those prepared in glycine buffer, pH 1.6. Next, the fibrils formed in concentrated ethanol solution had ~*ca.* 3 times greater diameters than those grown in acidic buffer. It is noteworthy that ethanol is capable of reducing the hydration of protein molecules [58, 69, 74]. In this regard, lysozyme molecules, being partially-denaturated by ethanol and the oxPLs dispersions, could transform into mature fibrils of similar morphology. Next, the difference spectra of CR showed the maxima at 542 nm in the presence of lysozyme aggregates formed by acidic denaturation (figure 5(A)), giving an additional evidence for amyloid nature of the observed structures. In turn, a weak CR absorption at 542 nm was detected in the presence of PazePC-triggered lysozyme fibrillization under near-physiological conditions, presumably being indicative of the formation of the large amount of the coil structure (figure 5(B)). Thus, the pronounced increase of ThT fluorescence could be explained by its higher specificity to the lysozyme fibrils prepared in the presence of PazePC dispersions, despite the lower extent of their formation compared to the aggregates grown in glycine buffer. In turn, the increase in ThT fluorescence with time of the protein incubation at pH 1.6, 60 °C, 16 μM

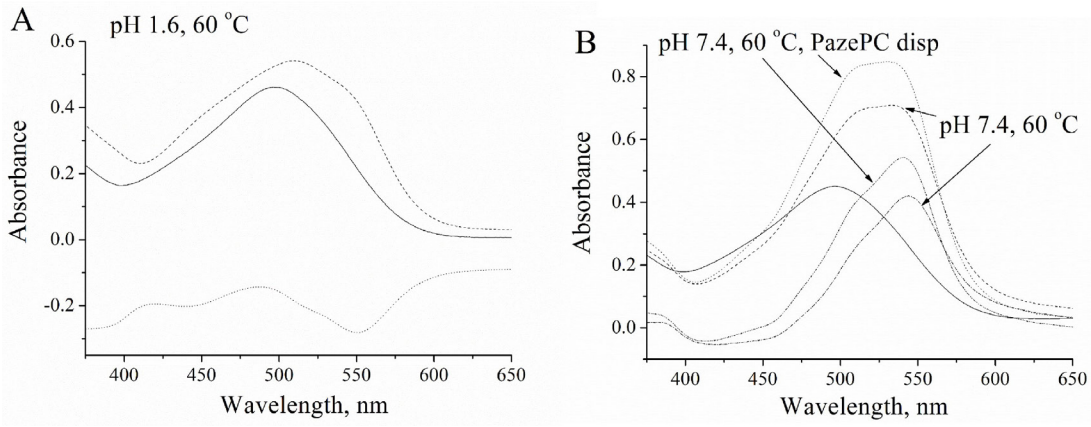

Figure 7. Absorption spectra of Congo Red (dashed lines) in the presence of fibrillar insulin prepared at 1.6, 60 °C (A), or pH 7.4, 60 °C, PazePC dispersion/pH 7.4, 60 °C (B). The spectra were corrected for light scattering due to fibrils. The dye and the protein concentrations were 48 and 33 μM, respectively. Solid lines correspond to the absorbance of free CR in buffer and dotted lines—to the difference spectra of CR.

Table 4. Kinetic parameters of insulin fibrillization in the presence of unoxidized and oxidized phospholipids.

Lipid type	pH	T (°C)	k (h^{-1})	lag time (h)	F_{max} (a.u.)	F_{max}/F_0, (a.u.)	$\Delta\lambda_{max}$ (nm)
Control	1.6	60	26	0.4	52	3	−10
PG_{20}			10	0.6	27	3	−5
PC			18	1.4	77	5	−10
$PazePC_{20}$			8	0.8	42	3	−5
$PoxnoPC_{20}$			6	0.6	37	2	−25
PoxnoPC disp			7	0.2	50	3	5
PazePC disp			6	0.3	40	3	−7
Control	7.4	37	0.4	2.9	97	6	−11
PG_{20}			1	2.8	117	7	−9
PC			0.6	4.5	144	8	−14
$PazePC_{20}$			0.5	2.7	136	8	−11
$PoxnoPC_{20}$			0.5	5.2	117	7	−11
PoxnoPC disp			0.4	7.3	143	8	−10
PazePC disp			0.6	6.1	399	23	−12
Control	7.4	60	5.5	0.2	285	16	−11
PG_{20}			5.3	0.5	293	17	−10
PC			2.5	0.4	172	10	−10
$PazePC_{20}$			4.4	0.3	303	17	−12
$PoxnoPC_{20}$			1.1	0.5	153	9	−11
PoxnoPC disp			1.9	0.5	334	19	−10
PazePC disp			2.9	0.5	457	26	−12

PazePC dispersions reveals the greater extent of fibril formation compared to that in the absence of lipid (figures 4(A) and (B)).

The above studies were further extended to gain insight into the oxPLs effect on insulin amyloid formation. Insulin is known to form amyloid fibrils at both the alkaline and acidic pH [61, 76]. Allowing for the low insulin solubility at pH 7.4, kinetic measurements were performed at the protein concentration of 1.6 μM. As seen in figure 6, the lowest values of F_{max} were observed for the aggregates grown at pH 1.6, 60 °C, irrespective to the lipid composition of vesicles/dispersions. Likewise, insulin adopts more amyloid-prone conformation at pH 7.4, being closer to its isoelectric point (pH 5.3) than the pH 1.6 [77]. Indeed, a weak CR absorption at 542 nm was observed in the presence of the aggregates grown at pH 1.6, 60 °C, being indicative of the large amount of the coil structure (figure 7(A)). Similar to lysozyme, the hypsochromic shifts of the ThT emission maxima with incubation time were found for insulin under the employed conditions. It appeared that membrane surfaces slow down insulin nucleation and elongation, in contrast to their effect on the extent of fibril formation (tables 1 and 4, lag time and k). The origin of this effect could be explained by the formation of highly stable lipid–protein complexes, hampering the production of insulin amyloid nuclei, as shown previously, e.g. for polyunsaturated docosahexaenoic fatty acid [78].

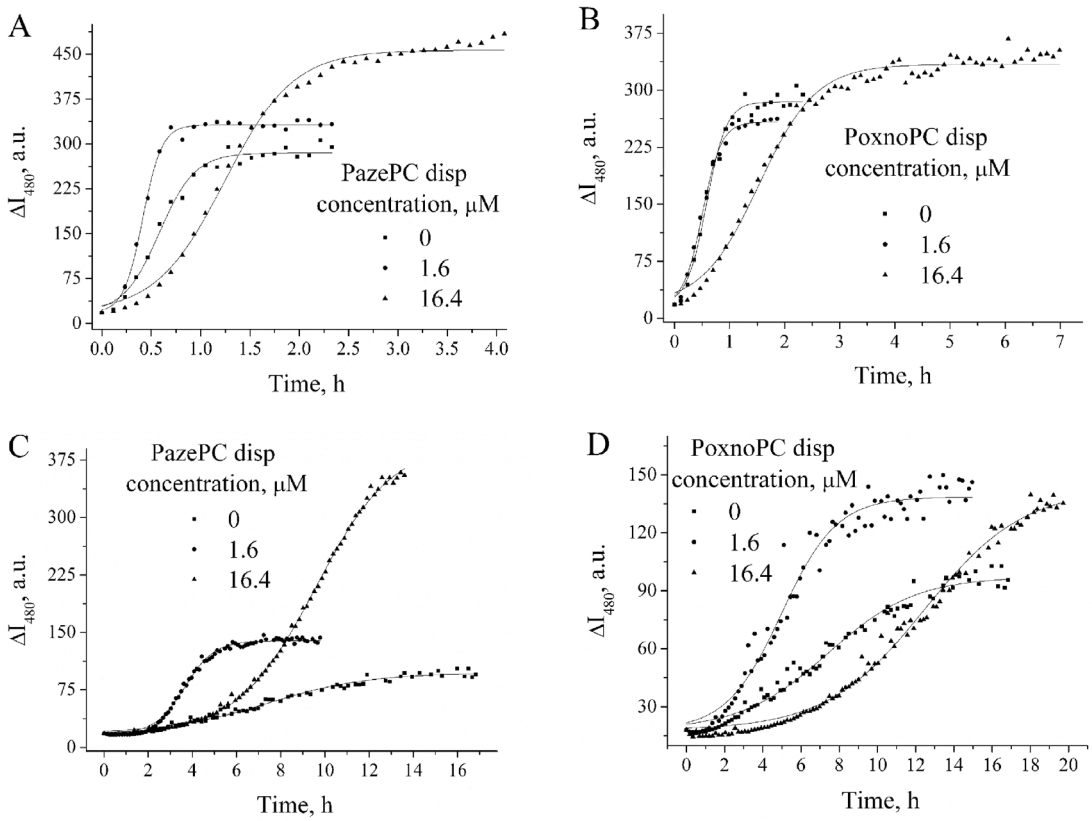

Figure 8. Kinetics of insulin fibrillization in the presence of the oxPLs dispersions at different lipid:protein ratios, pH 7.4, 130 mM NaCl, 60 °C ((A) and (B)) and pH 7.4, 130 mM NaCl, 37 °C ((C) and (D)). Insulin and ThT concentrations were 1.6 and 14 μM, respectively.

Again, in contrast to lysozyme, the lag times of insulin fibrillization in the presence of the oxPLs dispersions were ~*ca.* 2 times lower than those in control sample, probably due to the formation of the lipid-containing amyloid nuclei. Taking into consideration the fact that no significant incorporation of insulin molecules into the fluid mono-olein cubic phase was observed at pH 2, 60 °C, we can assume that van der Waals forces between double-chain lipids and proteins are stronger than those between the one-chain lipids and proteins [79]. In turn, lipids did not exhibit any pronounced effect on the extent of insulin amyloid formation.

At pH 7.4, 60 °C, we observed 2–5 times lower apparent rate constants for the insulin fibril growth compared to pH 1.6, 60 °C, consistent with the data obtained for lysozyme (tables 1 and 3). However, the lag times of amyloid formation in the presence of lipid vesicles were reduced up to 3.5 times at pH 7.4 compared to those at pH 1.6. This effect could be attributed to the decrease in stability of the lipid–protein complexes at pH 7.4 and the local increase in protein concentration. In turn, given that the lag times of insulin amyloid formation in the presence of the oxPLs dispersions were greater at pH 7.4, than at pH 1.6, the oxPLs premicellar aggregates could have a stabilizing effect on the protein oligomers at neutral pH that is consistent with the previous studies of gelsolin fragment [56]. This suggestion is further confirmed by the fact that the lag time and k were decreased at pH 7.4 relative to control sample. Finally, these results are consistent with the finding that lysozyme nucleation is enhanced in the presence of ionic surfactants at pH 7 [63]. However, F_{max} value of insulin fibrillization was increased in the presence of the oxPLs dispersions, compared to its value in the absence of lipids, although the PoxnoPC and PazePC had more pronounced effects on the kinetic parameters of lysozyme and insulin fibrillization (tables 1 and 4). Notably, the increase in ThT fluorescence with time of insulin incubation at pH 7.4, 60 °C, 16 μM PazePC dispersions reveals the enhanced number of mature fibrils, compared to that in the absence of lipid (figures 4(E) and (F)). The above results are corroborated by the stronger absorption of CR bound to the insulin aggregates grown in the presence of PazePC premicellar aggregates at 542 nm (figure 7(B)). Furthermore, $PoxnoPC_{20}$ vesicles inhibited insulin fibrillization at both the pH 7.4 and 1.6, while $PazePC_{20}$ vesicles did not affect the F_{max} values. Indeed, no substantial disruption of the oxPLs-containing vesicles was observed by DLS, because about *ca.* 80% of the fibril-bound liposomes had the same diameter, as that of the free vesicles (table 2). Notably, in the case of lysozyme, $PoxnoPC_{20}$ and $PazePC_{20}$ liposomes induced the decrease in the extent of fibril formation, compared to the fibril production in the presence of PC and PG_{20} vesicles. These effects could be attributed to the facilitated penetration of lysozyme

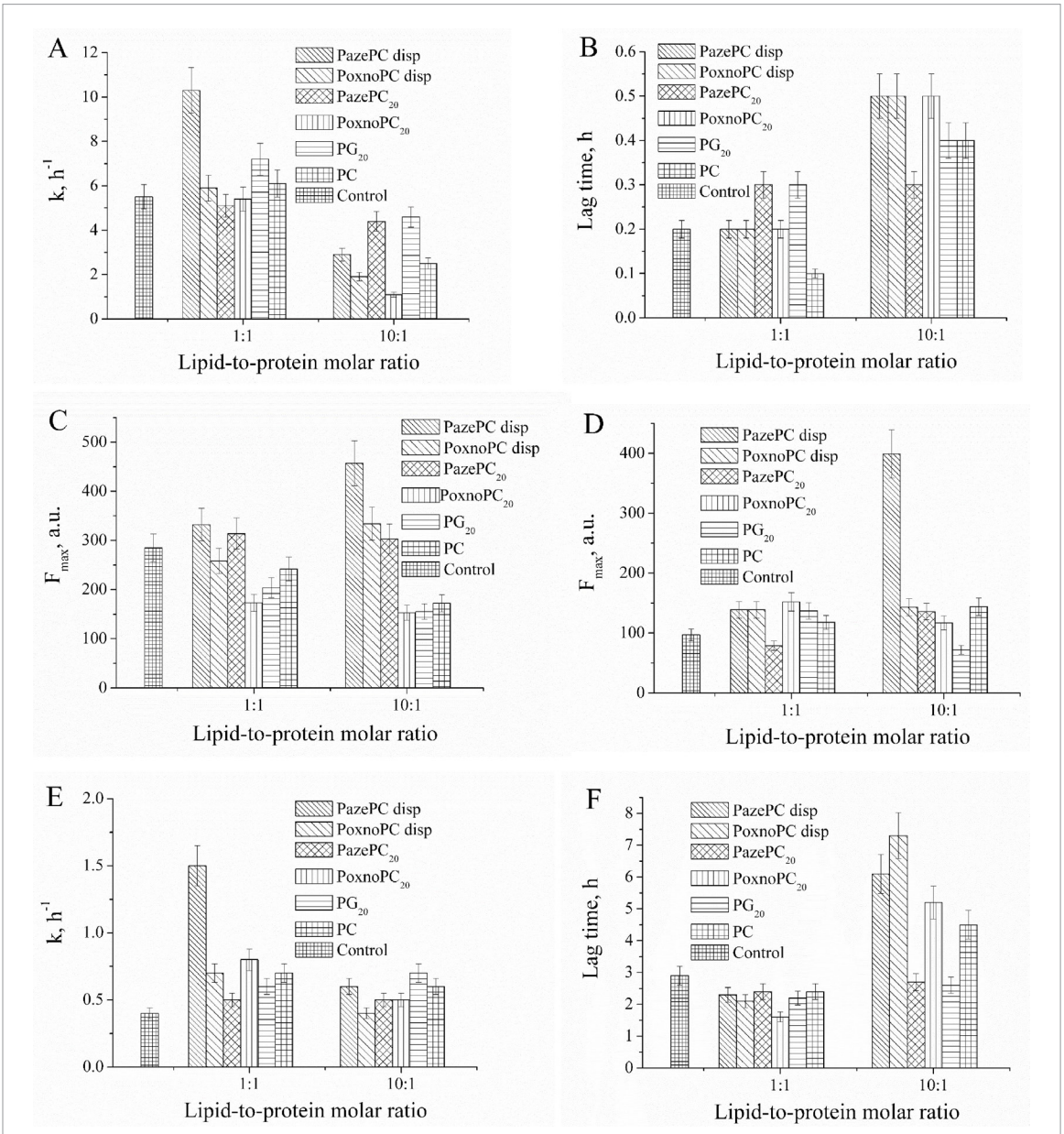

Figure 9. Kinetic parameters of lipid-modulated insulin fibrillization at pH 7.4, 130 mM NaCl, 14 μM ThT, 60 °C ((A)–(C)), and 37 °C ((D)–(F)). Protein concentration was 1.6 μM.

and insulin into the extended hydrophobic region of the oxPLs-containing membrane that slows down the interactions between hydrophobic (i.e. aggregation-prone) protein moieties [37, 46, 80]. PG_{20} vesicles did not induce a substantial change in the insulin fibrillization kinetics, in contrast to lysozyme, probably because the local decrease in pH was not essential for insulin aggregation under the employed experimental conditions. Furthermore, the lipid–protein hydrophobic interactions occurring in PC liposomes were followed by the distinct changes in F_{max} values relative to control at pH 1.6 and 7.4.

Since the highest extent of insulin fibrillization was observed at pH 7.4, the temperature effect on the lipid-modulated protein aggregation was further studied at pH 7.4 and 37 °C. Consistent with the results gained at 60 °C, similar values of k and F_{max} were found for the aggregates grown in the presence of liposomes, while the lag times were up to 2-fold longer than that in the control sample (table 4). Furthermore, the lag times and k were 9–15, 2–14 times greater at 37 °C, than at 60 °C, respectively, and F_{max} was 1.3–3 lower at 37 °C, than that at 60 °C. Thus, temperature and pH exert more pronounced effect on insulin fibrillization kinetics, than lipids. Again, at 37 °C the production of insulin fibrils increased in the presence of PazePC dispersions, which bear carbonyl group in its structure, relative to control. Notably, this effect did not show significant temperature dependence, unlike lysozyme. Furthermore, the dispersions of PazePC provoked a greater extent of insulin amyloid formation at pH 7.4, than that found in the presence of PoxnoPC premicellar aggregates, suggesting that the interaction of the carboxyl group of PazePC with insulin induces the highly aggregation-prone conformation of the protein.

Interestingly, our results were opposite to those, reported for micelles of amphiphilic surfactants that inhibited insulin fibrillization [81]. Specifically, Wang

and coworkers reported that the extent of insulin fibril formation at pH 2, 55 °C was ~6 times lower in the presence of the amphiphilic 1,2-diheptanoyl-sn-glycero-3-phosphocholine above the CMC than without lipid [46]. Furthermore, both the 1,2-dihexanoyl-sn-glycero-3-phosphocholine (DiC_6PC) and 1,2-diheptanoyl-sn-glycero-3-phosphocholine (DiC_7PC) surfactants exhibited the ability to suppress insulin and Aβ peptide fibrillization below the CMC at pH 2, 55 °C and 7, 25 °C, respectively [46, 81]. In contrast, our results showed that the oxPLs promoted insulin fibril formation at neutral pH and exerted no influence on this process under acidic conditions. These discrepancies can be explained by the differences in physicochemical properties and concentrations of the short-chain phospholipids and the oxPLs. First, protein interactions with the polar heads of the large DiC_7PC micelles with high polydispersity may alter the nucleation phase, exerting the stabilizing effect on the protein structure [83]. This hypothesis is further supported by the fact that ionic surfactants, sodium dodecyl sulfate and cetyltrimethylammonium bromide, above the CMC exerted similar inhibiting effects on lysozyme nucleation at pH 7, 55 °C [63]. Second, the enhanced amyloid fibril formation seems to be a result of the interactions between the oxPLs dispersions and hydrophobic surfaces of partially unfolded proteins [47, 56]. Furthermore, anionic detergents, containing alkyl chains of at least 12 carbons, formed micelles below the CMC in the presence of tau-protein, that was followed by the enhancement of tau fibrillization at pH 7, 37 °C [24]. The above considerations emphasize the important role of hydrophobic lipid–protein interactions in the amyloid fibril formation. Third, the short-chain phospholipids could induce membrane solubilization and release of integral membrane proteins due to the high affinity for the long-chain phospholipids [83]. These species also have parallel alignment of the two hydrocarbon chains in a micellar form, which is maintained in the monomeric state, as well. On the contrary, the oxPLs were reported to take only the extended conformation and reduce the polarity of the phospholipid heads [35, 36]. Such differences may lead to the opposite effects of the oxPLs and DiC_6PC, DiC_7PC surfactants below the CMC on the extent of insulin fibrillization [46]. Finally, insulin fibrils were prepared in our experiments at pH 7.4 in the presence of magnetic stirrers inside of the cuvette, while Wang and coworkers used pH 2 for fibril formation. These environmental conditions can modulate lipid effects on insulin fibrillization process and induce the differences in amyloid morphology. It should be noted that despite the opposite effect on the extent of fibril formation, the oxPLs and DiC_6PC, DiC_7PC surfactants inhibited the nucleation and elongation of insulin fibrils, presumably, due to the formation of highly stable lipid–protein complexes [46].

Finally, the effect of the lipid:protein ratio on insulin amyloid formation at pH 7.4 was investigated. Specifically, we performed additional studies of the protein fibrillization kinetics at lipid concentration 1.6 μM (figure 8). The kinetic parameters gained from these data are plotted in figure 9. It appeared that the lag time for insulin fibril formation increased proportionally to the amount of the oxPLs dispersions and PoxnoPC liposomes added, indicating the ability of the oxPLs to stabilize prefibrillar structures [56, 79]. Furthermore, this effect was stronger at 37 °C as compared to 60 °C, probably due to the formation of more stable lipid–protein complexes. The values of k were *ca.* 2 times lower at lipid:protein ratio 10:1, than those at lipid:protein ratio 1:1, suggesting that the oxPLs dispersions and $PoxnoPC_{20}$ liposomes inhibit amyloid elongation. However, at 37 °C, this effect remained significant only for the PazePC dispersions. Next, the increase of F_{max} was observed at higher lipid:protein ratio for the fibrils grown at 60 °C in the presence of the oxPLs dispersions, being more pronounced for PazePC premicellar aggregates at 37 °C. These observations can be interpreted as arising from the enhanced binding of the proteins to the oxPLs at high lipid concentration, resulting in the increased amount of the protein subjected to lipid-modulated nucleation. As was shown for islet amyloid polypeptide (IAPP), the highest rate of fibril formation on membrane surfaces from DOPG and DOPC, was observed for lipid:peptide molar ratio of 12:1, when IAPP was fully membrane-bound [23]. Indeed, the phospholipids below the CMC exerted a promoting effect on apolipoprotein C-II fibrillization, being proportional to the lipid:protein ratio [72]. In summary, the influence of the lipid:protein ratio on the extent of insulin fibrillization was the most pronounced for PazePC dispersions at 37 °C, compared to the PoxnoPC premicellar aggregates and the oxPLs-containing vesicles.

It should be noted that the effect of liposomes and lipid dispersions on the protein fibrillization was examined for the lipids in the fluid phase (which is the most important biologically) due to the very low temperature of POPC phase transition (~ −2 °C). The fluid phase (L_α) is characterized by the formation of kinks in unsaturated fatty acids, rapid lateral diffusion and flip-flop mechanisms [84, 85]. Furthermore, the temperature increase from 20 to 60 °C induced no substantial changes in the molecular organization of POPC bilayer. Specifically, the area per lipid raised from 62.7 to 68.1 Å^2, while the bilayer and hydrocarbon thickness decreased from 39.8 and 29.2 Å^2 to 37.7 and 28.0 Å^2, respectively [86]. On the contrary, the presence of 0.15 M NaCl reduced POPG area per lipid, allowing denser lipid packing due to the screening of electrostatic interactions [87]. Notably, POPC fluidity also decreased in the presence of 0.22 M NaCl, as well as upon the incorporation of POPG into POPC bilayer due to the smaller POPG area per lipid [87]. In turn, incorporation of the PoxnoPC and PazePC into POPC bilayer led to significant rise in fluidity and lipid phase segregation, because the reverse orientation of the oxidized chains created voids in the lipid matrix, resulting in the increased free volume of a membrane [36, 37]. It is very likely that the alterations in

fluidity affect the kinetics of the membrane-modulated amyloid fibril formation and the morphology of the protein aggregates. Indeed, as follows from the differential scanning calorimetry data, the lag time of Aβ-peptide fibrillization is shorter in liquid-ordered DPPC vesicles, containing cholesterol, than in solid DPPC liposomes [84]. On the contrary, a minor delay of the amyloid formation was detected in the presence of the fluid dioleoyl-phosphatidylcholine (DOPC) bilayers. However, the addition of NaCl induces the screening of Aβ repulsion, resulting in the peptide aggregation in the presence of liposomes in gel phase [84]. These results indicate that both high rate of lateral diffusion and highly ordered acyl chains represent the most favourable conditions for amyloid fibril formation. Therefore, the promoting effects of liposomes on the protein fibrillization may be observed if the incorporated protein enhances the order of chain packing in fluid membranes that requires its deeper insertion into the bilayer [88, 89]. The depth of the protein insertion into the fluid bilayer may increase at higher temperatures due to the increased area per lipid [86]. This process can also induce surface exposure of the protein hydrophobic patches, leading to the formation of the aggregation-prone states [84]. This is most likely, e.g. for lysozyme fibrillization in the presence of PC vesicles at pH 1.6, 37 °C and pH 1.6, 60 °C, because the stronger ThT fluorescence response was observed at 60 °C and no fibrils were formed in the control at 37 °C (table 1). Interestingly, the enhanced lateral mobility and flip-flop mechanisms in a fluid phase may trigger the segregation of negatively charged lipids, their migration to the outer leaflet, followed by the increase in the number of the membrane-adsorbed polycations [85, 90]. This effect is not expected to be crucial for the process of insulin and lysozyme aggregation due to their low surface charge density, although it may increase the number of Shiff-bases formed between the oxPLs and the proteins as compared to a gel phase. This could explain faster nucleation of lysozyme and insulin incorporated into $PoxnoPC_{20}$ or $PazePC_{20}$ bilayers at 60 °C than at 37 °C (tables 1 and 4). Finally, the most prominent effect of the oxPLs dispersions on lysozyme and insulin fibrillization at 60 °C, pH 1.6 and 7.4, respectively, as compared to that of liposomes, emphasizes the superiority of the high protein translational diffusion, allowing Shiff base and Michael adducts formation, versus the high order of the lipid acyl chains, allowing the enhanced van der Waals interactions.

4. Conclusion

Our fluorescence studies of lysozyme and insulin fibrillization kinetics in the presence the oxPLs support the following hypotheses. First, the oxPLs dispersions induce the increase in the extent of fibril formation compared to that in control samples and in the presence of liposomes composed of the oxidized and unoxidized phospholipids. Second, this effect is accompanied by the inhibition of the fibrillization kinetics by the oxPls premicellar aggregates, being more pronounced at high lipid concentrations, that indicates the oxPLs complexation with proteins and their stabilizing effect on the protein oligomers. Third, the oxPls dispersions may cause the variations in fibril morphology. Finally, the magnitude of the oxPLs effects is highly pH- and/or temperature-dependent, pointing to an essential role of these parameters in lysozyme and insulin fibrillization *in vitro*. Overall, the obtained results strongly suggest that oxidative stress may be implicated in the development of lysozyme and insulin-related amyloidoses.

Acknowledgments

This work was supported by CIMO Fellowship (KV).

Competing interests

The authors have declared that no competing interests exist.

References

[1] Caughey B and Lansbury P T 2003 Protofibrils, pores, fibrils, and neurodegeneration: separating the responsible protein aggregates from the innocent bystanders *Annu. Rev. Neurosci.* **26** 267–98
[2] Selkoe D J 2003 Folding proteins in fatal ways *Nature* **426** 900–4
[3] Sulatskaya A I, Kuznetsova I M and Turoverov K K 2011 Interaction of Thioflavin T with amyloid fibrils: stoichiometry and affinity of dye binding, absorption spectra of bound dye *J. Phys. Chem.* B **115** 11519–24
[4] Hudson S A, Ecroyd H, Kee T W and Carver J A 2009 The Thioflavin T fluorescence assay for amyloid fibril detection can be biased by the presence of exogenous compounds *FEBS J.* **276** 5960–72
[5] Groenning M 2010 Binding mode of Thioflavin T and other molecular probes in the context of amyloid fibrils—current status *J. Chem. Biol.* **3** 1–18
[6] Adachi E *et al* 2013 Dual role of an N-terminal amyloidogenic mutation in apolipoprotein A-I *J. Biol. Chem.* **288** 2848–56
[7] Mohanty J, Choudhury S D, Pal H and Bhasikuttan A C 2012 Early detection of insulin fibrillation: a fluorescence lifetime assay to probe the pre-fibrillar regime *Chem. Commun.* **48** 2403–5
[8] Sabaté R and Saupe S J 2007 Thioflavin T fluorescence anisotropy: an alternative technique for the study of amyloid aggregation *Biochem. Biophys. Res. Commun.* **360** 135–8
[9] Hobbs J R and Morgand O D 1963 Fluorescence microscopy with Thioflavine-T in the diagnosis of amyloid *J. Pathol. Bacteriol.* **86** 437–42
[10] Picken M M and Herrera G A 2012 Thioflavin T stain: an easier and more sensitive method for amyloid detection *Amyloid and Related Disorders* (Chicago, IL: Humana Press) pp 187–9
[11] Biancalana M, Makabe K, Koide A and Koide S 2009 Molecular mechanism of Thioflavin-T binding to the surface of β-rich peptide self-assemblies *J. Mol. Biol.* **385** 1052–63
[12] Stsiapura V I and Maskevich A A 2007 Computational study of Thioflavin T torsional relaxation in the excited state *J. Phys. Chem.* A **111** 4829–35
[13] Voropai E S *et al* 2003 Spectral properties of Thioflavin T and its complexes with amyloid fibrils *J. Appl. Spectrosc.* **70** 868–74
[14] Sulatskaya A I, Maskevich A A, Kuznetsova I M, Uversky V N and Turoverov K K 2010 Fluorescence quantum yield of Thioflavin T in rigid isotropic solution and incorporated into the amyloid fibrils *PLoS One* **5** e15385

[15] Biancalana M and Koide S 2010 Molecular mechanism of Thioflavin-T binding to amyloid fibrils *Biochim. Biophys. Acta* **1804** 1405–12
[16] Wu C, Biancalana M, Koide S and Shea J E 2009 Binding modes of Thioflavin-T to the single-layer beta-sheet of the peptide self-assembly mimics *J. Mol. Biol.* **394** 627–33
[17] Krebs M R, Bromley E H and Donald A M 2005 The binding of Thioflavin-T to amyloid fibrils: localisation and implications *J. Struct. Biol.* **149** 30–7
[18] Chothia C 1973 Conformation of twisted beta-pleated sheets in proteins *J. Mol. Biol.* **75** 295–302
[19] Stefani M 2008 Protein folding and misfolding on surfaces *Int. J. Mol. Sci.* **9** 2515–42
[20] Aisenbrey C, Borowik T, Byström R, Bokvist M, Lindström F, Misiak H, Sani M and Gröbner G 2008a How is protein aggregation in amyloidogenic diseases modulated by biological membranes? *Eur. Biophys. J.* **37** 247–55
[21] Jo E, Darabie A A, Han K, Tandon A, Frazer P E and McLaurin L 2004 α-synuclein—synaptosomal membrane interactions. Implications for fibrillogenesis *Eur. J. Biochem.* **271** 3180–9
[22] Bokvist M, Lindstrom F, Watts A and Grobner G 2004 Two types of Alzheimer's β-amyloid (1–40) peptide membrane interactions: aggregation preventing transmembrane anchoring versus accelerated surface fibril formation *J. Mol. Biol.* **335** 1039–49
[23] Knight J D and Miranker A D 2004 Phospholipid catalysis of diabetic amyloid assembly *J. Mol. Biol.* **341** 1175–87
[24] Chirita C N, Necula M and Kuret J 2003 Anionic micelles and vesicles induce tau fibrillization *in vitro J. Biol. Chem.* **278** 25644–50
[25] Zhao H, Tuominen E K J and Kinnunen P K J 2003 Formation of amyloid fibers triggered by phosphatidylserine-containing membranes *Biochemistry* **43** 10302–7
[26] Wang S S, Good T A and Rymer D L 2005 The influence of phospholipid membranes on bovine calcitonin peptide's secondary structure and induced neurotoxic effects *Int. J. Biochem. Cell. Biol.* **37** 1656–69
[27] Kazlauskaite J, Sanghera N, Sylvester I, Venien-Bryan C and Pinheiro T J T 2003 Structural changes of the prion protein in lipid membranes leading to aggregation and fibrillization *Biochemistry* **42** 3295–304
[28] Berliner J A, Subbanagounder G, Leitinger N, Watson A D and Vora D 2001 Evidence for a role of phospholipid oxidation products in atherogenesis *Trends Cardiovasc. Med.* **11** 142–7
[29] Tsimikas S, Brilakis E S, Miller E R, McConnell J P, Lennon R J, Kornman K S, Witztum J L and Berger P B 2005 Oxidized phospholipids, Lp(a) lipoprotein, and coronary artery disease *New Engl. J. Med.* **353** 46–57
[30] Berliner J A and Watson A D 2005 A role for oxidized phospholipids in atherosclerosis *New Engl. J. Med.* **353** 9–11
[31] Fruhwirth G O, Loidl A and Hermetter A 2007 Oxidized phospholipids: from molecular properties to disease *Biochim. Biophys. Acta* **1772** 718–36
[32] Mattila J P, Sabatini K and Kinnunen P K J 2007 Oxidized phospholipids as potential novel drug targets *Biophys. J.* **93** 3105–12
[33] Rosen M J and Liu L 1996 Surface activity and premicellar aggregation of some novel diquaternary gemini surfactants *J. Am. Oil Chem. Soc.* **73** 885–90
[34] Cwiklik L and Jungwirth P 2010 Massive oxidation of phospholipid membranes leads to pore creation and bilayer disintegration *Chem. Phys. Lett.* **486** 99–103
[35] Volinsky R, Cwiklik L, Jurkiewicz P, Hof M, Jungwirth P and Kinnunen P K J 2011 Oxidized phosphatidylcholines facilitate phospholipid flip-flop in liposomes *Biophys. J.* **101** 1376–84
[36] Sabatini K, Mattila J P, Megli F M and Kinnunen P K 2006 Characterization of two oxidatively modified phospholipids in mixed monolayers with DPPC *Biophys. J.* **90** 4488–99
[37] Volinsky R and Kinnunen P K 2013 Oxidized phosphatidylcholines in membrane-level cellular signaling: from biophysics to physiology and molecular pathology *FEBS J.* **280** 2806–16
[38] Megli F M, Russo L and Sabatini K 2005 Oxidized phospholipids induce phase separation in lipid vesicles *FEBS Lett.* **579** 4577–84
[39] Sayre L M, Perry G and Smith M A 2008 Oxidative stress and neurotoxicity *Chem. Res. Toxicol.* **21** 172–88
[40] Perry G, Cash A D and Smith M A 2002 Alzheimer disease and oxidative stress *J. Biomed. Biotechnol.* **2** 120–3
[41] Jenner P 2003 Oxidative stress in Parkinson's disease *Ann. Neurol.* **53** S26–36
[42] Smith M A, Hirai K, Hsiao K, Pappolla M, Harris P L R, Siedlak S L, Tabaton M and Perry J 1998 Amyloid-β deposition in Alzheimer transgenic mice is associated with oxidative stress *J. Neurochem.* **70** 2212–15
[43] Hashimoto M, Hsu L J, Xia Y, Takeda A, Sisk A, Sundsmo M and Masliah E 1999 Oxidative stress induces amyloid-like aggregate formation of NACP/α-synuclein *in vitro* *Neuroreport* **10** 717–21
[44] Alies B, Hureau C and Faller P 2013 The role of metal ions in amyloid formation: general principles from model peptides *Metallomics* **5** 183–92
[45] Bolognin S, Messori L, Drago D, Gabbiani C, Cendron L and Zatta P 2011 Aluminum, copper, iron and zinc differentially alter amyloid-A1–42 aggregation and toxicity *Int. J. Biochem. Cell. Biol.* **43** 877–85
[46] Koppaka V and Axelsen P H 2000 Accelerated accumulation of amyloid beta proteins on oxidatively damaged lipid membranes *Biochemistry* **39** 10011–6
[47] Kinnunen P K, Kaarniranta K and Mahalka A K 2012 Protein-oxidized phospholipid interactions in cellular signaling for cell death: from biophysics to clinical correlations *Biochim. Biophys. Acta* **1818** 2446–55
[48] Bieschke J, Zhang Q, Bosco D A, Lerner R A, Powers E T, Wentworth P Jr and Kelly J W 2006 Small molecule oxidation products trigger disease-associated protein misfolding *Acc. Chem. Res.* **39** 611–9
[49] Sayre L M, Smith M A and Perry G 2001 Chemistry and biochemistry of oxidative stress in neurodegenerative disease *Curr. Med. Chem.* **8** 721–38
[50] Trusova V M *et al* 2010 Förster resonance energy transfer evidence for lysozyme oligomerization in lipid environment *J. Phys. Chem.* B **114** 16773–82
[51] Kinnunen P K J 2009 Amyloid formation on lipid membrane surfaces *Open Biol. J.* **2** 163–75
[52] Campioni S *et al* 2010 A causative link between the structure of aberrant protein oligomers and their toxicity *Nat. Chem. Biol.* **6** 140–7
[53] van Rooijen B D, Claessens M M A E and Subramaniam V 2010 Membrane permeabilization by oligomeric a-synuclein: in search of the mechanism 2010 *PLoS One* **5** e1429
[54] Demuro A, Mina E, Kayed R, Milton S C, Parker I and Glabe C G 2005 Calcium dysregulation and membrane disruption as a ubiquitous neurotoxic mechanism of soluble amyloid oligomers *J. Biol. Chem.* **280** 17294–300
[55] Valincius G, Heinrich F and Budvytyte R 2008 Soluble amyloid β-oligomers affect dielectric membrane properties by bilayer insertion and domain formation: implications for cell toxicity *Biophys. J.* **95** 4845–61
[56] Mahalka A K, Maury C P J and Kinnunen P K J 2011 1-palmitoyl-2-(90-oxononanoyl)-sn-glycero-3-phosphocholine, an oxidized phospholipid, accelerates finnish type familial gelsolin amyloidosis *in vitro Biochemistry* **50** 4877–89
[57] Klunk W E 1989 Quantitative evaluation of Congo Red binding to amyloid-like proteins with a beta-pleated sheet conformation *J. Histochem. Cytochem.* **37** 1273–81
[58] Goda S 2000 Amyloid protofilament formation of hen egg lysozyme in highly concentrated ethanol solution *Protein Sci.* **9** 369–75
[59] Morozova-Roche L A, Zurdo J, Spencer A, Noppe W, Receveur V, Archer D B, Joniau M and Dobson C M 2000 Amyloid fibril formation and seeding by wild-type human lysozyme and its disease-related mutational variants *J. Struct. Biol.* **30** 339–51
[60] Arnaudov L N and de Vries R 2005 Thermally induced fibrillar aggregation of hen egg white lysozyme *Biophys. J.* **88** 515–26

[61] Kachooei E, Moosavi-Movahedi A A, Khodagholi F, Ramshini H, Shaerzadeh F and Sheibani N 2012 Oligomeric forms of insulin amyloid aggregation disrupt outgrowth and complexity of neuron-like PC_{12} cells *PLoS One* **7** e41344
[62] Nielsen L, Khurana R, Coats A, Frokjaer S, Brange J, Vyas S, Uversky V N and Fink A L 2001 Effect of environmental factors on the kinetics of insulin fibril formation: elucidation of the molecular mechanism *Biochemistry* **40** 6036–46
[63] Kumar E K and Prabhu N P 2014 Differential effects of ionic and non-ionic surfactants on lysozyme fibrillation *Phys. Chem. Chem. Phys.* **16** 24076–88
[64] Dusa A, Kaylor J, Edridge S, Bodner N, Hong D P and Fink A L 2006 Characterization of oligomers during α-synuclein aggregation using intrinsic tryptophan fluorescence *Biochemistry* **45** 2752–60
[65] Navarra G, Tinti A, Leone M, Militello V and Torreggiani A 2009 Influence of metal ions on thermal aggregation of bovine serum albumin: aggregation kinetics and structural change *J. Inorg. Biochem.* **103** 1729–38
[66] Beranova L, Cwiklik L, Jurkiewicz P, Hof M and Jungwirth P 2010 Oxidation changes physical properties of phospholipid bilayers: fluorescence spectroscopy and molecular simulations *Langmuir* **26** 6140–4
[67] Ioffe V M, Gorbenko G P, Domanov Y A, Tatarets A L, Patsenker L D, Terpetsching E A and Dyubko T S 2006 A new fluorescent squaraine probe for the measurement of membrane polarity *J. Fluoresc.* **16** 47–52
[68] Lindberg D J, Wranne M S, Gilbert Gatty M, Westerlund F and Esbjörner E K 2015 Steady-state and time-resolved Thioflavin-T fluorescence can report on morphological differences in amyloid fibrils formed by Aβ(1–40) and Aβ(1–42) *Biochem. Biophys. Res. Commun.* **458** 418–23
[69] Holley M, Eginton C, Schaefer D and Brown L R 2008 Characterization of amyloidogenesis of hen egg lysozyme in concentrated ethanol solution *Biochem. Biophys. Res. Commun.* **373** 164–8
[70] Vernaglia B A, Huang J and Clark E D 2004 Guanidine hydrochloride can induce amyloid fibril formation from hen egg-white lysozyme *Biomacromolecules* **5** 1362–70
[71] Raudino A and Castelli F 1992 A thermodynamic study of protein–lipid lateral phase separation. Effect of lysozyme on mixed lipid vesicles *Coll. Polym. Sci.* **270** 1116–23
[72] Hung A, Griffin M D, Howlett G J and Yarovsky I 2008 Effects of oxidation, pH and lipids on amyloidogenic peptide structure: implications for fibril formation? *Eur. Biophys. J.* **38** 99–110
[73] Bochkov V N, Oskolkova O V, Birukov K G, Levonen A-L, Binder C J and Stöck J 2010 Generation and biological activities of oxidized phospholipids *Antioxid. Redox Signal.* **12** 1009–59
[74] Yonezawa Y, Tanaka S, Kubota T, Wakabayashi K, Yutani K and Fujiwara S 2002 An insight into the pathway of the amyloid fibril formation of hen egg white lysozyme obtained from a small-angle x-ray and neutron scattering study *J. Mol. Biol.* **323** 237–51
[75] Vus K, Trusova V, Gorbenko G, Sood R, Kirilova E, Kirilov G, Kalnina I and Kinnunen P 2014 Fluorescence investigation of interactions between novel benzanthrone dyes and lysozyme amyloid fibrils *J. Fluoresc.* **24** 493–504
[76] Tiiman A, Noormägi A, Friedemann M, Krishtal J, Palumaa P and Tõugu V 2013 Effect of agitation on the peptide fibrillization: Alzheimer's amyloid-β peptide 1–42 but not amylin and insulin fibrils can grow under quiescent conditions *J. Pept. Sci.* **19** 386–91
[77] Schmittschmitt J P and Scholtz J M 2003 The role of protein stability, solubility, and net charge in amyloid fibril formation *Protein Sci.* **12** 2374–78
[78] Johansson A S, Garlind A, Berglind-Dehlin F, Karlsson G, Edwards K, Gellerfors P, Ekholm-Pettersson F, Palmblad J and Lannfelt L 2007 Docosahexaenoic acid stabilizes soluble amyloid-β protofibrils and sustains amyloid-β-induced neurotoxicity *in vitro FEBS J.* **274** 990–1000
[79] Kraineva J, Smirnovas V and Winter R 2007 Effects of lipid confinement on insulin stability and amyloid formation *Langmuir* **23** 7118–26
[80] Gorbenko G P and Kinnunen P K 2006 The role of lipid–protein interactions in amyloid-type protein fibril formation *Chem. Phys. Lipids* **141** 72–82
[81] Wang S S-S, Liu K-N and Han T-C 2010 Amyloid fibrillation and cytotoxicity of insulin are inhibited by the amphiphilic surfactants *Biochim. Biophys. Acta* **1802** 519–30
[82] Wang S S-S, Chen Y-T and Chou S-W 2005 Inhibition of amyloid fibril formation of h-amyloid peptides via the amphiphilic surfactants *Biochim. Biophys. Acta* **1508** 164–81
[83] Hauser H 2000 Short-chain phospholipids as detergents *Biochim. Biophys. Acta* **1741** 307–13
[84] Hellstrand E, Sparr E and Linse S 2010 Retardation of A β fibril formation by phospholipid vesicles depends on membrane phase behavior *Biophys J.* **98** 2206–14
[85] Yaroslavov A A, Kuchenkova O Y, Okuneva I B, Melik-Nubarov N S, Kozlova N O, Lobyshev V I, Menger F M and Kabanov V A 2003 Effect of polylysine on transformations and permeability of negative vesicular membranes *Biochim. Biophys. Acta* **1611** 44–54
[86] Kučerka N, Nieh M P and Katsaras J 2011 Fluid phase lipid areas and bilayer thicknesses of commonly used phosphatidylcholines as a function of temperature *Biochim. Biophys. Acta* **1808** 2761–71
[87] Shoemaker S D and Vanderlick T K 2002 Intramembrane electrostatic interactions destabilize lipid vesicles *Biophys. J.* **83** 2007–14
[88] Sasahara K, Morigaki K and Shinya K 2013 Effects of membrane interation and aggregation on amyloid β-peptide mobility and membrane domain structure *Phys. Chem. Chem. Phys.* **15** 8929–39
[89] Kremer J J, Pallitto M M, Sklansky D J and Murphy R M 2000 Correlation of beta-amyloid aggregate size and hydrophobicity with decreased bilayer fluidity of model membranes *Biochemistry* **39** 10309–18
[90] Volodkin D, Ball V, Schaaf P, Voegel J C and Mohwald H 2007 Complexation of phosphocholine liposomes with polylysine. Stabilization by surface coverage versus aggregation *Biochim. Biophys. Acta* **768** 280–90